Theoretical and experimental study of micropolar elastic materials using acoustic waves in air

Erick Ogam, Zine El Abiddine Fellah, Mohamed Fellah, Claude Depollier

Theoretical and Experimental study of micropolar elastic materials using acoustic waves in air

Erick Ogam[a,*], Zine El Abbidine Fellah[a], Mohamed Fellah[b], Claude Depollier[c]

[a] *Laboratoire de Mécanique et d'Acoustique LMA - UMR 7031 AMU - CNRS - Centrale Marseille*
[b] *Laboratoire de physique théorique, Faculté de physique, Université des Sciences et de la Technologie Houari Boumediene, BP 32 El Alia 16111 Bab Ezzouar Alger, Algeria.*
[c] *Laboratoire d'Acoustique de l'Université du Mans - UMR CNRS 6613 (LAUM), Avenue Olivier Messiaen 72085 - Le Mans cedex 9 France.*

Abstract

This study focuses on the development of a theoretical and experimental acoustic method and setup for studying the micropolar behavior of materials. Two types of low density closed-cell foams made from polystyrene (expanded and extruded) materials that were previously reported as materials exhibiting the non-classical elastodynamic behavior were investigated in order to reveal the particular comportment using acoustic waves. Two different types of transducers were employed to provide a large frequency band to study the influence of the Cosserat parameters. The frequency band from 1-40 kHz was covered using a twitter loudspeaker whereas that from 30-120 kHz, by an air coupled ultrasonic transducer. The materials' micropolar elastic behavior were revealed through the comparison between the theoretical and experimental transmission coefficients. At the cut-off frequency where the theoretical phase velocity of the transverse acoustic mode was established to be infinite, the acoustic wave transmission by the panels was found to be very small. This makes the Cosserat materials appealing to harmonic noise reduction.

Keywords: Micropolar elasticity, Acoustic transmission coefficient, Air-filled closed-cell foams, cut-off frequency, Recovery of Cosserat parameters

*Principal corresponding author
Email address: ogam@lma.cnrs-mrs.fr (Erick Ogam)

1. Introduction

The Cosserat brothers, Eugène and François, published a monograph [1] in 1909 in which they presented a new variant of Continuum Mechanics. This detailed treatise covered the idea of taking into account additionally the couple stresses, the rotational degrees of freedom (micro-rotations) and their gradients of the material particles as independent variables. The existence of the couple stresses was originally postulated by Voigt in 1887 [2].

The couple stress theory using macrorotation as the true kinematical rotation for elastic bodies in which the gradient of the rotation vector is used as a curvature tensor was developed much later by Toupin [3], Mindlin and Tiersten [4], Koiter [5]. These formulations use the four foundational continuum mechanical quantities (i.e., force, displacement, couple, rotation) and are the fundamental pillars in the development of size-dependent continuum mechanics. Heterogeneous materials exhibit intrinsic material length scales (like in cellular structures, grains, particles and fibers). However, these formulations pose some challenges like the indeterminacy of the spherical part of the couple-stress tensor and the appearance of the body couple in the constitutive relation for the force-stress tensor [4, 6]. Hadjesfandiari and Dargush [7] resolved the inconsistencies by revealing the subtle skew-symmetric character of the couple-stress tensor and showed that it was a true vector. The constrained Cosserat theory is a particular case of the couple stress theory in which kinematic constraints have been introduced in order to eliminate some of the degrees of freedom [8] in order to obtain a simpler system of equations.

The extension of the linear Cosserat theory to include body microinertia effects is attributed to Eringen[9]. He is also the one who renamed it as the micropolar theory of elasticity [10]. A complete variant of this theory can be found in Kafadar and Eringen [11]. Micropolar continuum mechanics [12] therefore incorporates a local rotation of points (micropolar continua in the sense of Eringen) including the translation assumed in classical elasticity; and a couple stress as well as the force stress.

Six material parameters are needed in the linear micropolar elasticity of isotropic

solids while only two Lamé moduli are necessary in the classical elasticity. A review and survey of the literature on the theory of Cosserat continuum can be found in [13, 14]. This theory has been extended further to capture more complex micropolar material behavior [15–17].

The majority of studies pertaining to the micropolar elastodynamics of materials have been mainly theoretical. The most popular media geometry studied was that of an infinite half-plane corresponding to the ground in geology and seismic studies. Many of the problems reported were those concerning reflection and refraction of plane waves at plane interfaces in which seismic waves generated within a semi-infinite half-plane micropolar solid media interact with, for example, a viscous liquid layer [18, 19]. The few experimental measurements reported were mainly undertaken using mechanical (static, quasi-static) means [20–23]. All six elastic constant parameters (like the apparent shear modulus) have been found from torque and twist measurements in a pure torsion experiment using a circular cylinder and the cylindrical bending of a rectangular plate [24].

In this study, a theoretical micropolar elastic model was developed and employed to validate a new experimental method to study acoustic wave transmission through air-filled closed-cell polystyrene panels considered to obey Cosserat elasticity (micropolar continuum theory) law. The frequency domain ranges from the audible to the ultrasonic regimes but < 120 kHz. The foams studied were two-phase composite materials in which one phase was solid and the other, fluid (air). In this case, the size scale is large, the material may no longer be assumed to be continuous [25, 26]. A table in reference [14] classified the closed-cell polystyrene foams in the family of Cosserat elasticity materials. The micropolar continuum theory model considered herein was that of the generalized plane strain conditions assuming that the strain distributions do not depend on the third coordinate geometry of the acoustic wave transmission through panels experiment. The other reason motivating this study is that elastic data for closed-cell materials like the EPS and XPS foams are hard to come by in the literature and the only existing methods used by manufacturers are based on the static destructive mechanical methods declined

as standard test methods [27, 28].

2. Theoretical and experimental methods

2.1. Theoretical method for wave propagation in a Cosserat continuum

The loadings on a micropolar continuum of density ρ and rotational inertia J generate deformation of the body described by the displacement vector $\mathbf{u}$ and the rotation vector $\boldsymbol{\Phi}$.

The equations of motion in the micropolar elastic continuum are [20, 29]

$$(\lambda + 2\,\mu + \mathcal{K})\,\nabla(\nabla \bullet \mathbf{u}) - (\mu + \mathcal{K})\,\nabla \times (\nabla \times \mathbf{u}) + \mathcal{K}\nabla \times \boldsymbol{\Phi} - \rho\,\frac{\mathrm{d}^2}{\mathrm{d}t^2}\mathbf{u} = 0,$$

$$(\alpha + \beta + \gamma)\,\nabla(\nabla \bullet \boldsymbol{\Phi}) - \gamma\,\nabla \times \nabla \times \boldsymbol{\Phi} + \mathcal{K}\,\nabla \times \mathbf{u} - 2\,\mathcal{K}\,\boldsymbol{\Phi} - \rho\,J\frac{\mathrm{d}^2}{\mathrm{d}t^2}\boldsymbol{\Phi} = 0, \qquad (1)$$

where λ, μ are the Lamé constants, α, β, $\mathcal{K}$ and γ are the new elastic constants usually referred to as the micropolar or Cosserat elastic constants.

In order to uncouple the equations of motion in Eqn. (1), the Helmholtz decomposition is employed i.e., decompose the vectors $\boldsymbol{u}$ and $\boldsymbol{\Phi}$ into their potential and solenoidal parts

$$\begin{aligned} \boldsymbol{u} &= \nabla q + \nabla \times \boldsymbol{\Pi}, \quad \nabla \bullet \boldsymbol{\Pi} = 0, \\ \boldsymbol{\Phi} &= \nabla \xi + \nabla \times \boldsymbol{\Theta}, \quad \nabla \bullet \Theta = 0, \end{aligned} \qquad (2)$$

The following uncoupled wave equations for the potentials q and ξ are obtained

$$\begin{aligned} c_1^2\,\nabla^2 q - \frac{\partial^2}{\partial t^2} q &= 0, \\ c_3^2\,\nabla \xi - \omega_0^2 \xi - \frac{\partial^2}{\partial t^2}\xi &= 0, \end{aligned} \qquad (3)$$

where $c_1^2 = \frac{\lambda+2\,\mu+\mathcal{K}}{\rho} = \frac{M+\mathcal{K}}{\rho}$, $c_3^2 = \frac{\alpha+\beta+\gamma}{\rho\, J}$, $\omega_0^2 = \frac{2\mathcal{K}}{\rho J}$.

The coupled system of wave propagation equations for the determination of the vector potential for $\boldsymbol{\Pi}$ and $\boldsymbol{\Theta}$

$$\begin{aligned} c_2^2\,\nabla^2\boldsymbol{\Pi} + \frac{J\omega_0^2}{2}\nabla\times\boldsymbol{\Theta} - \frac{\boldsymbol{\partial^2}}{\boldsymbol{\partial t^2}}\boldsymbol{\Pi} &= 0, \\ c_4^2\,\nabla^2\boldsymbol{\Theta} - \omega_0^2\Theta + \frac{\omega_0^2}{2}\,\nabla\times\boldsymbol{\Pi} - \frac{\partial^2}{\partial t^2}\boldsymbol{\Theta} &= 0. \end{aligned} \tag{4}$$

where $c_2^2 = \frac{\mu+\mathcal{K}}{\rho}$, $c_4^2 = \frac{\gamma}{\rho J}$,

These equations govern the propagation of waves travelling in a Cosserat continuum.

The details of deriving the dispersion relations are found in the Appendix A or in [30].

Finally, there are four different waves propagating with four different phase velocities

$$v_1^2 = c_1^2 = \frac{\lambda+2\mu+\mathcal{K}}{\rho}, \qquad v_2^2 = {c_3}^2 + \frac{{\omega_0}^2}{k^2}, \qquad v_{3,4}^2 = \frac{\omega^2}{k_{3,4}^2}. \tag{5}$$

Therefore, in a micropolar elastic medium of infinite extent propagates four types of modes, 1) A longitudinal displacement wave mode propagating with a phase velocity, v_1 also called Longitudinal Acoustic mode (LA-mode), 2) A longitudinal microrotation wave (L0-mode) propagates with the velocity v_2, 3) Transverse acoustic mode (TA-mode), propagating with phase velocity v_3, 4) Transverse Optic mode (TO-mode) propagating with phase velocity v_4.

It can be shown that the velocity of the longitudinal microrotation wave (v_2) is dispersive (depends on frequency) when $\omega > \sqrt{2}\omega_0$

$$v_2^2 = \frac{\alpha+\beta+\gamma}{J\rho(1-\frac{2\omega_0^2}{\omega^2})}. \tag{6}$$

However, when $\omega = \omega_c = \sqrt{2}\omega_0$, v_2 is infinite and the wave number equals zero.

When $\omega < \omega_c$, v_2 is purely imaginary. The characteristic frequency ω_c acts as a

cut-off frequency below which the wave number vanishes.

The TO velocity $v_3 = \infty$ at $\omega = \omega_c$. The sketches of the phase velocities v_3 and v_4 are given in reference [29]. It was shown that at $\omega = \omega_c$, $v_3 = \infty$. For $\omega < \omega_c^-$, $v_3 = -\infty$ and at $\omega > \omega_c^+$, $v_3 = +\infty$. The transverse optic mode wave velocity v_4 is finite over the whole frequency range.

The experimental analysis of the phenomenon occuring around the cut-off frequency of v_3 was therefore of significant interest in this study.

2.2. Plane strain problem geometry and boundary equations

The direct problem of acoustic wave transmission by a micropolar elastic panel was simplified into a plane strain one. The objective consisted in determining the transmission coefficient in a two dimensional setup in which a known plane wave impinged on the boundary of an infinite micropolar elastic panel of finite thickness. In this configuration, the panel is bounded on both sides by a fluid (air) of semi-infinite extent (Fig. 1).

A simple two dimensional problem where displacement $\boldsymbol{u}$ and rotation $\boldsymbol{\Phi}$ fields depend only on two space variables u_y, u_z and Φ_x and the time t was studied (Fig. 1). In this case the field equations can be decomposed into an independent set (plane strain) with

$$\boldsymbol{u} = (0, u_y, u_z), \qquad \boldsymbol{\Phi} = (\Phi_x, 0, 0), \quad \partial/\partial x = 0.$$

An incident acoustic plane wave propagating in the fluid Ω_0 impinges on the panel at an incident angle θ and is reflected at the $z = 0$ plane at the boundary Γ_1. Mode transformation takes place i.e, from longitudinal wave in the fluid into the four micropolar elastic wave modes (LA, TA, LO and TO wave modes) in the panel. Multiple internal reflections of one of the modes within the layer is also represented in Fig. (1) for only a single mode for clarity.

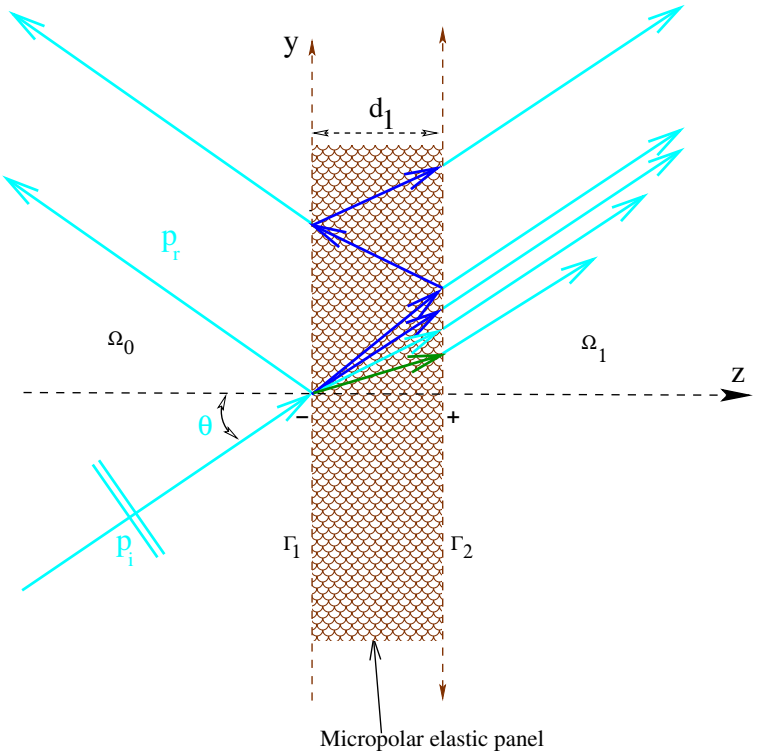

Figure 1: Geometry of the acoustic wave transmission problem. The panel is supposed to extend to infinity in the positive and negative y - directions.

2.2.1. The boundary conditions

The boundary surface Γ_1 and Γ_2 are free from traction and couples, the equations for the boundary conditions for transmission/reflection through an infinite extent micropolar plate immersed in air. The stress tensors σ_{zz}, σ_{yz} and the couple stress tensor m_{yz} are employed

$$\begin{aligned}
\sigma_{zz}(y,z) &= \lambda\left(\frac{\partial^2}{\partial y^2}q\left(y,z\right)+\frac{\partial^2}{\partial z^2}q\left(y,z\right)\right)+\left(2\,\mu+\mathcal{K}\right)\left(\frac{\partial^2}{\partial z^2}q\left(y,z\right)-\frac{\partial^2}{\partial z\partial y}\Pi_x\left(y,z\right)\right),\\
\sigma_{zy}(y,z) &= \left(2\,\mu+\mathcal{K}\right)\frac{\partial^2}{\partial z\partial y}q\left(y,z\right)+\left(\mu+\mathcal{K}\right)\frac{\partial^2}{\partial z^2}\Pi_x\left(y,z\right)-\mu\,\frac{\partial^2}{\partial y^2}\Pi_x\left(y,z\right)+\\
&\quad \mathcal{K}\left(\frac{\partial}{\partial y}\Theta_z\left(y,z\right)-\frac{\partial}{\partial z}\Theta_y\left(y,z\right)\right),\\
m_{zx}(y,z) &= \gamma\left(\frac{\partial^2}{\partial z\partial y}\Theta_z\left(y,z\right)-\frac{\partial^2}{\partial z^2}\Theta_y\left(y,z\right)\right).
\end{aligned}\tag{7}$$

The continuity of the acoustic particle velocity at the boundaries of the panel $\Gamma_{1,}$ and $\Gamma_{2,}$ are also sought. The velocity in the panel is given by

$$v_z\left(y,z\right)=\mathrm{i}\omega\frac{\partial}{\partial z}q\left(y,z\right)-\mathrm{i}\omega\frac{\partial}{\partial y}\Pi_x\left(y,z\right)\qquad z\geq\Gamma_{1,}\cup z\leq\Gamma_2,$$

The 8 boundary conditions' equations are set using the following stress, torque and velocity equations

$$\begin{aligned}
\sigma_{zz}(y,0) &= -p_I,\ \ z\in\Gamma_{1,},\ \sigma_{zz}(y,d_1)=-p_T\ \ z\in\Gamma_2,\\
\sigma_{zy}(y,0) &= 0,\ \ z\in\Gamma_{1,},\ \sigma_{zy}(y,d_1)=0\ \ z\in\Gamma_2,\\
m_{yz}(y,z) &= 0,\qquad z\in\Gamma_1\cup\Gamma_2,\\
v_z^{\Gamma_{1+}}\left(y,0\right) &= v_z^{\Gamma_{1-}}\left(y,0\right),\qquad v_z^{\Gamma_{2+}}\left(y,d_1\right)=v_z^{\Gamma_{2-}}\left(y,d_1\right).
\end{aligned}\tag{8}$$

The acoustic pressure in the fluid medium at $z\leq\Gamma_1$ (p_I) and at $z\geq\Gamma_{2,}$ (p_T) are

given by

$$\begin{aligned} p_I(y,z) &= P_I \left(\mathrm{e}^{\kappa_z^f z} + R\mathrm{e}^{-\kappa_z^f z} \right) \mathrm{e}^{\kappa_y^f y}, z \leq \Gamma_1, \\ p_T(y,z) &= T\, P_I\, \mathrm{e}^{(\kappa_{z1}+\kappa_{z3}+\kappa_{z4})d_1 + \kappa_z^f (z-d_1)}\, \mathrm{e}^{\kappa_y^f y}, z \geq \Gamma_2, \end{aligned} \tag{9}$$

where R and T are the reflection and transmission coefficients respectively, $\kappa_z^f = \frac{\mathrm{i}\omega}{c_f} \cos(\theta_I)$ (θ_I is the oblique angle of incidence), $\kappa_y^f = \frac{\mathrm{i}\omega}{c_f} \sin(\theta_I)$, c_f is the acoustic wave velocity in the fluid. The wave velocities are computed using the expressions of the fluid pressure above and the linear Euler equation, $v_z(y,z) = \dfrac{-1}{\mathrm{i}\omega\, \rho_f} \dfrac{\partial}{\partial\, z} p(y,z)$. The complex wave numbers $\kappa_{zn} = \mathrm{i}k_n \cos(\theta_n)$ (n= 1 ... 4) for the waves propagating in the micropolar elastic panel.

The incident and reflected waves are indicated by superscripts I and R propagate in the slab. The potentials for the micropolar elastic medium are given by

$$q = a_1^I \exp\left[\mathrm{i}k_1 \left(\sin\theta_1^I y + \cos\theta_1^I z\right) - i\omega_1^I t\right] + a_1^R \exp\left[\mathrm{i}k_1 \left(\sin\theta_1^R y - \cos\theta_1^R z\right) - \mathrm{i}\omega_1^R t\right], \tag{10}$$

$$\begin{aligned} \Pi_x = A_{3x}^I \exp\left[\mathrm{i}k_3 \left(\sin\theta_3^I y + cos\,\theta_3^I z\right) - \mathrm{i}\omega_3^I t\right] + A_{3x}^R \exp\left[\mathrm{i}k_3 \left(\sin\theta_3^R y - \cos\theta_3^R z\right) - \mathrm{i}\omega_3^R t\right] + \\ A_{4x}^I \exp\left[\mathrm{i}k_4 \left(\sin\theta_4^I y + \cos\theta_4^I z\right) - \mathrm{i}\omega_4^I t\right] + A_{4x}^R \exp\left[\mathrm{i}k_4 \left(\sin\theta_4^R y - \cos\theta_4^R z\right) - \mathrm{i}\omega_4^R t\right], \end{aligned} \tag{11}$$

Since the transverse TA and TO waves are coupled we can write

$$\begin{aligned} \Theta_y = \eta_{3y} \left\{ A_{3x}^I \exp\left[\mathrm{i}k_3 \left(\sin\theta_3^I y + \cos\theta_3^I z\right) - \mathrm{i}\omega_3^I t\right] + A_{3x}^R \exp\left[\mathrm{i}k_3 \left(\sin\theta_3^R y - \cos\theta_3^R z\right) - \mathrm{i}\omega_3^R t\right] \right\} + \\ \eta_{4y} \left\{ A_{4x}^I \exp\left[\mathrm{i}k_4 \left(\sin\theta_4^I y + \cos\theta_4^I z\right) - \mathrm{i}\omega_4^I t\right] + A_{4x}^R \exp\left[\mathrm{i}k_4 \left(\sin\theta_4^R y - \cos\theta_4^R z\right) - \mathrm{i}\omega_4^R t\right] \right\} \end{aligned} \tag{12}$$

$$\Theta_z = \eta_{3z}\left\{A_{3x}^I \exp\left[\mathrm{i}k_3\left(\sin\theta_3^I y + \cos\theta_3^I z\right) - \mathrm{i}\omega_3^I t\right] + A_{3x}^R \exp\left[\mathrm{i}k_3\left(\sin\theta_3^R y - \cos\theta_3^R z\right) - \mathrm{i}\omega_3^R t\right]\right\} +$$
$$\eta_{4z}\left\{A_{4x}^I \exp\left[\mathrm{i}k_4\left(\sin\theta_4^I y + \cos\theta_4^I z\right) - \mathrm{i}\omega_4^I t\right] + A_{4x} \exp\left[\mathrm{i}k_4\left(\sin\theta_4^R y - \cos\theta_4^R z\right) - \mathrm{i}\omega_4^R t\right]\right\}, \tag{13}$$

where the coupling coefficients $\eta_{3,4}$ were derived from Eqn. (A.3) using the amplitude ratios

$$\bar{\mathbf{\Theta}}_y = \frac{-\mathrm{i}\omega_0^2}{2\left(\omega^2 - \omega_0^2 - c_4^2 k^2\right)} k_z \bar{\Pi}_x, \qquad \bar{\mathbf{\Theta}}_z = \frac{\mathrm{i}\omega_0^2}{2\left(\omega^2 - \omega_0^2 - c_4^2 k^2\right)} k_y \bar{\Pi}_x, \tag{14}$$

and finally the amplitude ratios

$$\eta_{3,4y} = -\frac{\mathrm{i}\omega_0^2}{2\,k_{3,4}(v_{3,4}^2 - \frac{\omega_0^2}{k_{3,4}^2} - c_4^2)} \cos\theta_{3,4}, \qquad \eta_{3,4z} = \frac{\mathrm{i}\omega_0^2}{2\,k_{3,4}(v_{3,4}^2 - \frac{\omega_0^2}{k_{3,4}^2} - c_4^2)} \sin\theta_{3,4}, \tag{15}$$

The complex wave-numbers $\kappa_f = \mathrm{i}\vartheta_f$, $\vartheta_f = k_f sin(\theta_I)$ (k_f is the compressional wave number in the fluid). Simplifications can be done on the potentials by writing $\theta_n^I = \theta_n^R$ ($n = 1 \ldots 4$). The complex wave numbers $\kappa_{zn} = \mathrm{i}k_n \cos(\theta_n)$ for the four waves propagating in the micropolar elastic panel are related to the incident wave number in the fluid through Snell-Descartes law of refraction and therefore can be written

$$\begin{aligned} \kappa_{z1} &= \mathrm{i}\sqrt{k_1^2 - \vartheta_f^2}, \quad \kappa_{z2} = \mathrm{i}\sqrt{k_2^2 - \vartheta_f^2} \\ \kappa_{z3} &= \mathrm{i}\sqrt{k_3^2 - \vartheta_f^2}, \quad \kappa_{z4} = \mathrm{i}\sqrt{k_4^2 - \vartheta_f^2} \end{aligned} \tag{16}$$

The hysteretic model of inherent damping of the panels were taken into account by introducing a scalar-valued loss factor $\chi(\omega)$ into Young's modulus [31], such that $E_d(\omega) = E_r(\omega) + \mathrm{i}E_i(\omega) = E(\omega)(1 + \mathrm{i}\chi(\omega))$ ($E_r(\omega)$ is called the storage modulus and $E_i(\omega)$ the loss modulus of the panel, $M(\omega) = \frac{E(\omega)(1-\nu)}{(1+\nu)(1-2\nu)}$ where ν is the Poisson ratio). $E(\omega)$ is approximately constant in the chosen bandwidth (there is a basic lag between the stress and the strain and therefore the area of the hysteresis cycle does not depend on the frequency of the harmonic motion). The relationships between the different elastic

moduli can be found in reference [32].

A matrix equation is deduced from the 8 boundary conditions' equations

$$\begin{bmatrix} s\kappa_{z1} & -sk_{z1} & \cdots & -\frac{P_i\cos(\theta_I)}{c_f\,\rho_f} & 0 \\ & & & & \\ & & \vdots & & \vdots \\ & & & & \\ 0 & 0 & \gamma\left(\eta_{3z}\kappa_f\kappa_{z3}-\eta_{3y}\kappa_{z3}^2\right) & \cdots & 0 & 0 \end{bmatrix} \times \begin{bmatrix} a_{1I} \\ a_{1R} \\ A_{3xI} \\ A_{3xR} \\ A_{4xI} \\ A_{4xR} \\ R \\ T \end{bmatrix} = \begin{bmatrix} -\frac{P_i\cos(\theta_I)}{c_f\,\rho_f} \\ 0 \\ -P_i \\ 0 \\ 0 \\ 0 \\ 0 \\ 0 \end{bmatrix},$$

where $s = i\omega$.

The matrix equation is written as a linear system in the form $\boldsymbol{Ax} = \boldsymbol{b}$ ($\boldsymbol{A}$ is an 8×8 matrix) and the equation solved to obtain T or R.

2.3. Materials, experimental method and setup

Expanded polystyrene (EPS) and Extruded polystyrene (XPS) are air-filled (95-98%) closed-cell rigid foams [33] panels of different thicknesses were employed. These are two types of foams of the same material (polystyrene) but are manufactured differently. EPS is made from beads that are molded or cut into various sizes and shapes while XPS is made from extruded sheets [33].

The experimental setup is shown in Fig. 2. A transient pulse wave was generated using a loudspeaker driven by a waveform function generator (Agilent 33250B, Loveland Colorado, USA) through a power amplifier Bruel and Kjaer (B&K2706, Naerum Denmark). The excitation signal generated was a positive rectangular pulse. The Fourier transform of the excitation pulse $g(t)$ with amplitude A and width P_{wdt} in seconds is

$$G(f) = A\,P_{wdt}\,sinc(\pi f P_{wdt}). \tag{17}$$

As P_{wdt} becomes very large, the magnitude spectrum approaches a Dirac delta function located at the origin. As the height of the pulse becomes higher and its width smaller, it approaches a Dirac delta function and the magnitude spectrum flattens out and becomes a constant. This latter case results in a signal with large frequency band-width being generated. Shorter pulse widths also avoid the risk of damaging the loud-speaker when the amplitude is high. When the panel is thin, the first mode has a high frequency value, therefore, P_{wdt} is smaller, and relatively wider for a thick panel. The pulse width was chosen $5\,\mu s < P_{wdt} < 12\,\mu s$. Even though the generated pulse is rectangular form, the captured pulse of the incident wave will look sinusoidal because the generator signal output is convoluted with the response of the loud-speaker.

The chosen loudspeaker was a Visaton (GmbH, Haan, Germany) magnetostatic ribbon tweeter reference MHT 12 - 8 Ohm with an opening, 60 mm wide and $\times$ 84 mm high. It was selected among several others because it had a low distortion factor, good power-handling capabilities (100 Watts), highly linear impedance and amplitude frequency response and a broad frequency response range (1 kHz - 50kHz). This is the first time such a tweeter speaker is being employed in this frequency range. This wide range is an advantage over the non-contact air-coupled ultrasonic transducers that are band limited around their central working frequency e.g the Ultran NCG50-S50 (State College, PA USA) is a 50kHz center frequency transducer whose band-with is $\approx$ 20 kHz.

The transmitted acoustic wave was captured using a small (1/8 inch) pressure-field condenser microphone (Type B&K4138 , Naerum Denmark) connected to a frequency analyzer (B&K2120, Naerum Denmark). The very low noise and high amplification analyzer was used in the measuring microphone amplifier mode (2 Hz - 200kHz). The signals from the microphone amplifier were then digitized using a Tektronix oscilloscope model TDS3014B (Beaverton, OR USA). The transmission coefficient was obtained by calculating the transfer function estimate between the captured incident acoustic pressure(obtained without the panel in place). The transmitted acoustic pressure was acquired when the panel was placed perpendicularly between the acoustic source and the

sensor (microphone).

The transmission coefficient was computed as a transfer function of a linear time-invariant (LTI) system giving the ratio between the incident pressure and the transmitted acoustic pressure. The transmission coefficient $T(f)$ was obtained from the quotient of the cross spectral power density S_{it} (between the incident, $p_i(t)$ and the transmitted, $p_t(t)$) acoustic pressure) and the auto-spectral power density S_{ii} ($p_i(t)$),

$$\tilde{T}(f) = \frac{\tilde{S}_{it}(f)}{\tilde{S}_{ii}(f)}. \tag{18}$$

where the tilde ($\sim$) indicates that the function is an estimate only. The quotient $\tilde{T}(f)$ was calculated in Matlab® employing the function *tfestimate* [34] using the acquired signals. In order to avoid spectral leakage and attain accurate spectral measurements, the temporal signals were first windowed [35].

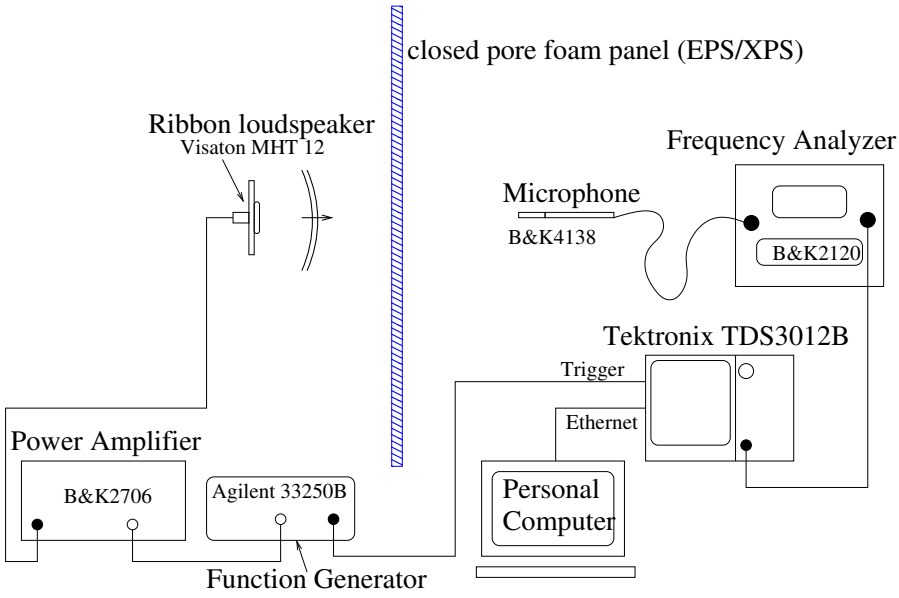

Figure 2: The experimental setup for the acoustic wave transmission by a panel.

Using a 50 kHz ultrasonic transducer as acoustic source to extend the measurement bandwidth

The measurement frequency bandwidth beyond 40 kHz was extended by replacing the loudspeaker by an air-coupled ultrasonic probe as an acoustic excitation source [36]. The exciter probe (Ultran NCG50-S50, State College, PA USA) had a center frequency at 50 kHz and was connected to a Panametrics 5058-PR (Waltham USA) pulser. The replacement of the acoustic exciter just modified the experimental setup slightly as the acoustic receiver remained the same as in the loudspeaker source/microphone configuration. If the ultrasonic detector had been used as receiver in place of the microphone, it would have engendered undesirable reflections from its non-negligible larger surface area rendering the modeling more complex. It was actually found to reflect the transmitted waves backwards towards the panels due to its large surface area. The NCG50-S50 has a large (50 mm $\times$ 50 mm) active area. This is the reason why a tiny 1/8 inch in diameter B&K 4138 microphone was preferred as receiver/detector.

3. Results

3.1. XPS Panels

The temporal signals representing the incident pressure (without the 4cm thick XPS panel) and transmitted pressure (with the panel placed between the speaker and the microphone) and their frequency spectrum are depicted in Figs. (3)a and b, respectively. A rectangular window providing a better spectral accuracy was employed during the signal processing.

From the zoomed view of the temporal signals (Fig. (3)a), it can be noticed that the transmitted acoustic pressure wave is attenuated but arrives at the microphone position earlier than the incident waves. This is because the acoustic waves travel faster in the micropolar elastic solid than in air and are therefore accelerated in a small portion of the solid panel layer.

The frequency spectrum depicted in Fig. (3)b shows that the spectrum of the transmitted pressure wave is cut-off at around 5-6 kHz (calculated ω_c is 5319 Hz such that the amplitude is diminished around this frequency value. The comparison between the theoretical micropolar elastic model and the experimentally determined transmission coefficients (TC) are shown in Fig. (3)c. The theoretical cut-off frequency f_c is ≈5319 Hz.

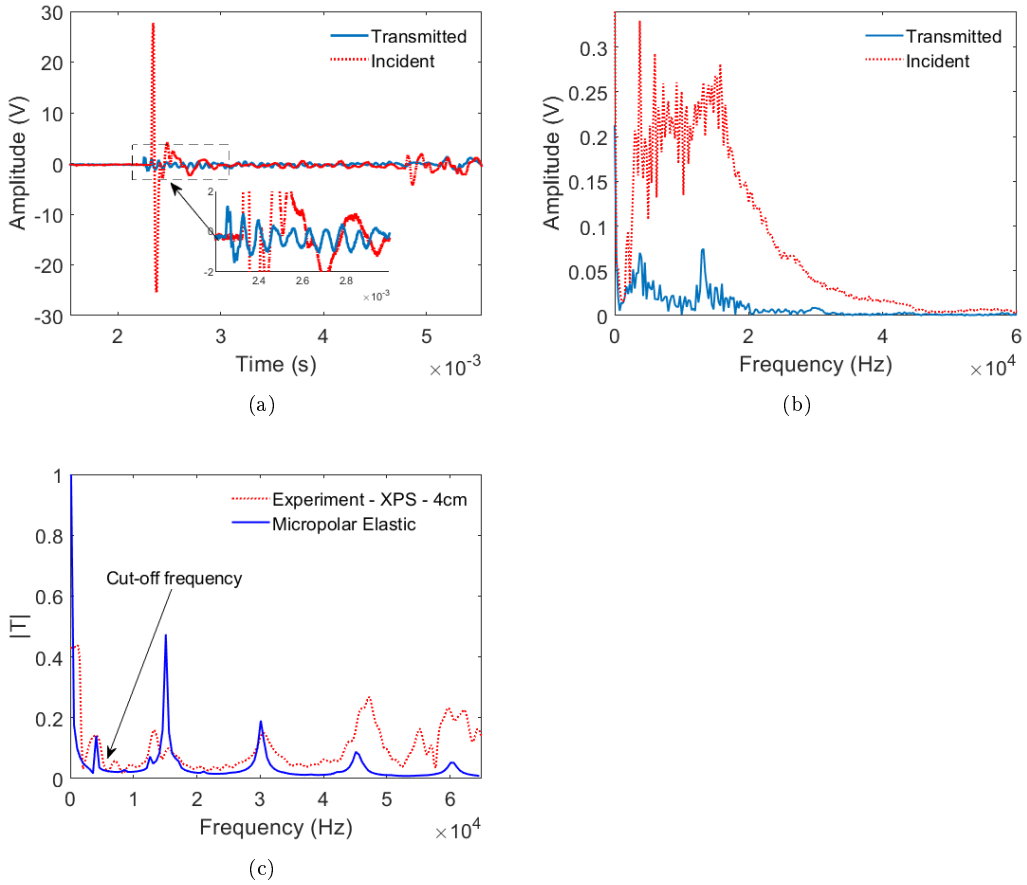

Figure 3: For the 4.0 cm thick XPS panel, (a) The temporal signals representing the incident and transmitted pressure. The transmitted wave is attenuated, albeit faster than the incident wave. (b) The frequency spectrum. Comparisons between the theoretical micropolar elastic and classical elastic models with experimental data (c) transmission coefficients. The computed cut-off frequency is at 5319 Hz.

The measurements results for the 2.0 cm thick XPS panel are shown in Fig. (4)a -

c. It can be noted that the frequency of the modes also depend on the thickness of the panel. The thicker the panel, the lower the frequency values of the modes.

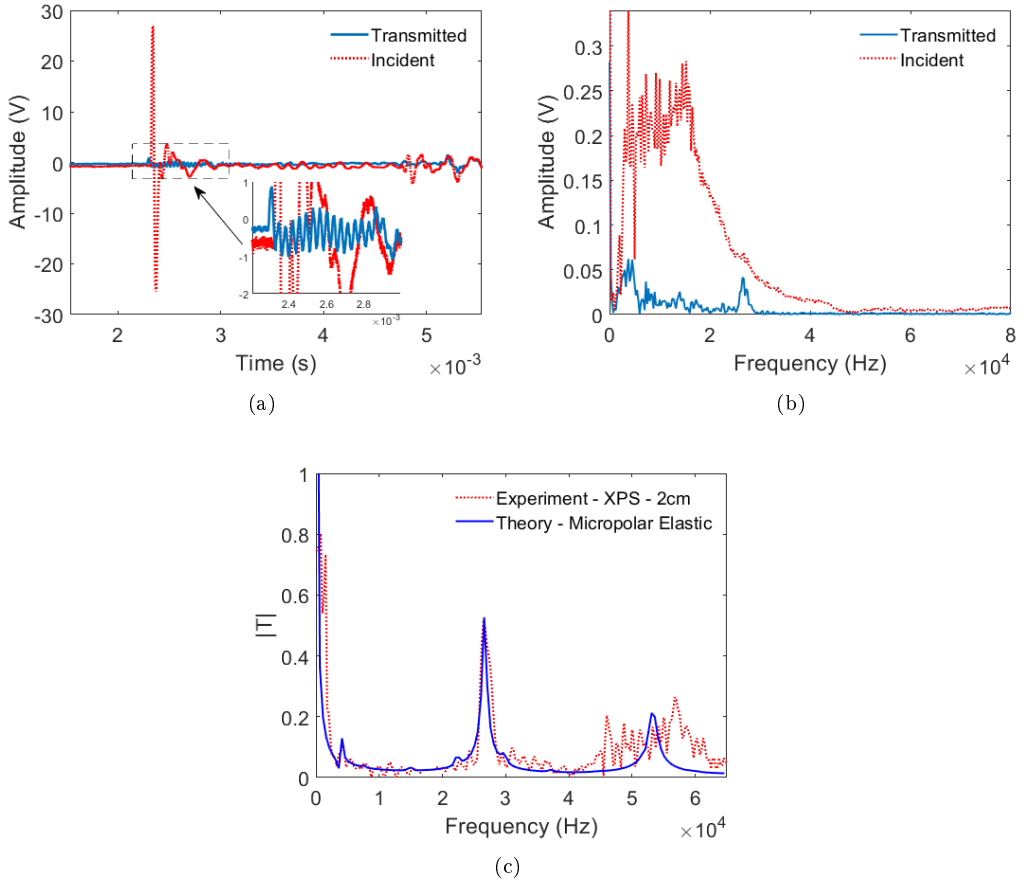

Figure 4: For the 2.0 cm thick XPS panel.(a) The temporal signals representing the incident and transmitted pressure (b) Their frequency spectrum. Comparisons between the theoretical and experimental, (c) the corresponding transmission coefficient.

3.2. EPS12 Panel

The results for the 2 cm thick EPS12 panels are shown in Fig. (5)a - c and the transmission coefficient for the 3 cm panel, in Fig. (5)d (the theoretical cut-off frequencies, $f_{c_{2\,cm}} = 2171$ Hz and $f_{c_{3\,cm}} = 3071$ Hz). The transmission coefficient dips at the cut-off frequency (velocity of the transverse acoustic mode is ∞). The frequency of the first peak representing the first mode in the EPS12 panel is lower than that of the XPS panel

of the same thickness (Fig. 4c and Fig. 5c) meaning that the values of its micropolar and elastic moduli are lower.

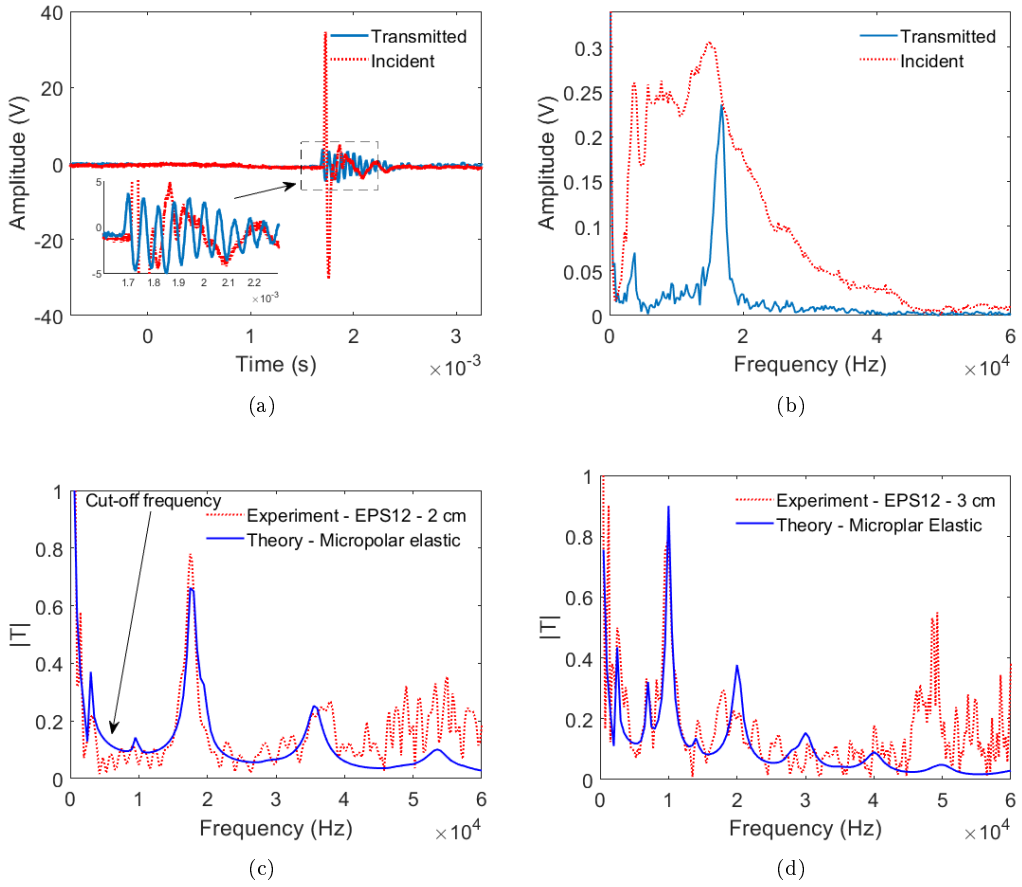

Figure 5: For the 2.0 cm thick EPS12 panel, (a) The temporal signals representing the incident and transmitted pressure (b) Their frequency spectrum. (c) Comparisons between the theoretical and experimental transmission coefficients. (d) The transmission coefficient for the 3.0 cm thick EPS12 panel

The test results for an EPS12 4.0 cm thick panel are shown in Fig. fig:A-4cm-thick xps panelc, (6). The acceleration (or early arrival) of the acoustic wave transmitted by the layer as compared to the incident acoustic pressure is more remarkable on the temporal signal of this panel, even without zooming.

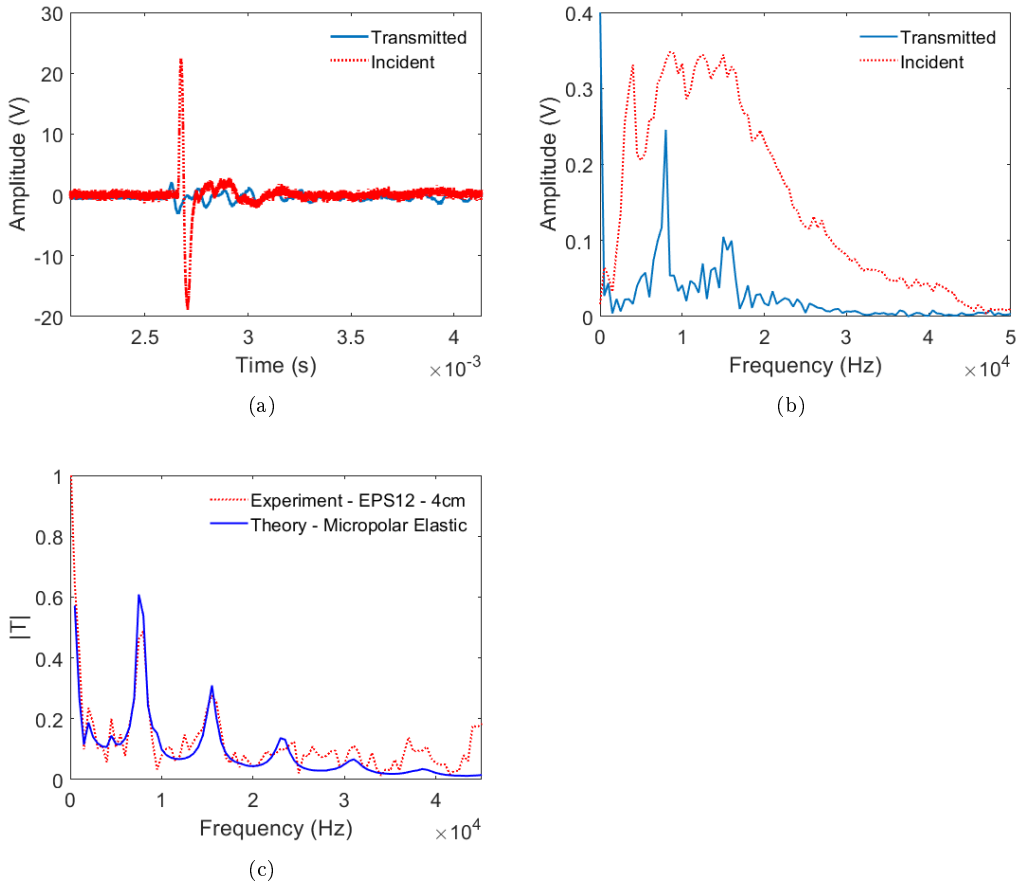

Figure 6: For the 4.0 cm thick EPS12 panel, (a) The temporal signals representing the incident and transmitted pressure (b) Their frequency spectrum. (c) Comparisons between the theoretical and experimental transmission coefficients.

Extended bandwidth using a 50 kHz ultrasonic transducer as acoustic exciter source

The frequency band covered by the ribbon twitter loudspeaker was from 2 - ≈35 kHz (see Figs. 3c, 4c, 5c and d, 6c). The peaks of the modes were not well marked beyond that bandwidth due to the low signal to noise ratio (SNR). This was due to the limited bandwidth of the loudspeaker. The SNR were lower for the thicker panels. In order to cover the higher frequencies following i.e, from ≈ 30-90 kHz, an air coupled ultrasonic transducer was employed in place of the loudspeaker.

The incident temporal acoustic wave pressure signals and the comparison between the

captured experimental and the computed theoretical transmission coefficients are shown in Fig. (7). The spectra corresponding to the temporal signals are shown in Fig. (7)b. The transmission coefficient is shown in Fig. (7)(c). The acoustic modes up to 120 kHz are excited by this transducer and captured by the microphone. The transducer response covers the high frequency zones where the loudspeaker response is lower, however, the lower frequencies are not well reproduced with the former. The situation is improved when the loudspeaker is employed because of its superior frequency response in the lower frequency range.

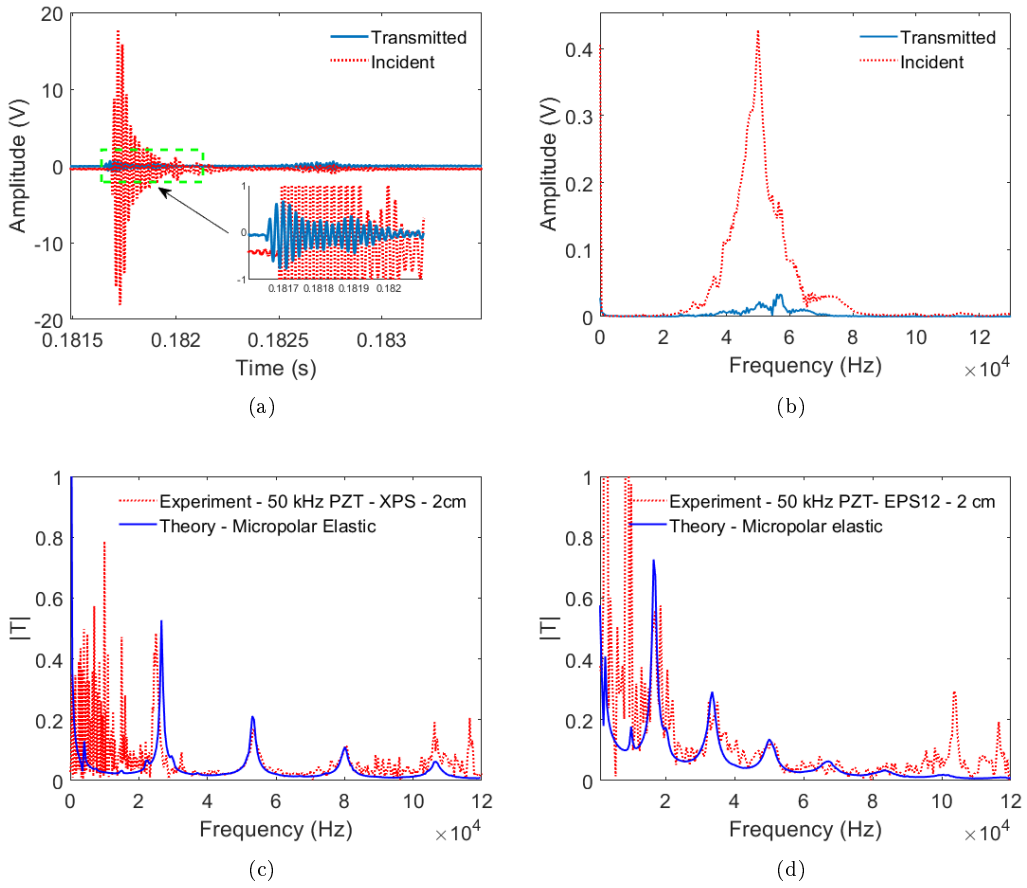

Figure 7: Using an Ultran air-coupled PZT transducer as acoustic source to probe a 2.0 cm XPS panel, (a) The incident and transmitted acoustic waves in the time domain, (b) Their spectrum. (c) Comparison between the theoretical and experimental transmission coefficients. (d) TC for the 2 cm thick EPS12 panel.

Table 1: Adjusted parameters employed in the theoretical model to fit the experimental curves. The microinertia is J.

Panel	d_1 (cm)	ρ (kg/m^3)	E (MPa)	Loss χ	ν	$\mathcal{K}$ (MPa)	γ (MN)	J (N/m)
XPS	2	32	2.7	0.02	0.49	0.0510	1.68	2.35e-5
XPS	4	32	2.8	0.02	0.49	0.0510	0.57	2.35e-5
EPS12	2	12	1.4	0.06	0.45	0.070	0.86	3.13e-5
EPS12	3	12	1.5	0.06	0.43	0.070	1.2	3.13e-5
EPS12	4	12	1.2	0.075	0.45	0.037	0.87	3.9e-5

4. Discussion

4.1. Comparison between the Young's modulus recovered with those obtained using other methods

A summary of the micropolar parameters for the problem are tabulated in Table (1). The precise optimized values will be given in a future study involving the resolution of a complete inverse problem for wave propagation in Cosserat elastic continuum. A Manufacturer of EPS12 foams under the name of Geofoam (ACH Foam Technologies® (Denver, CO USA)), Geofoams (AFM Corporation®, Lakeville, MN USA) indicates that the Elastic modulus measured using the ASTM D6817 standard [27, 28] at a compression of 1% is 1500 (kPa). Reference [37] also reports that the initial tangent modulus (determined from the linear portion of the stress-strain curve [37, 38]) for EPS12 is 1600 kPa. These compare well with the value obtained from the experiment. The advantage of the acoustic method is that it is non destructive and is lower compression rate as compared to the Compression test methods where the materials are cut in cylindrical, rectangular and cube form.

4.2. Phase wave velocities as a means of verification of some of the material parameters

The phase wave velocity of the P-wave modes (numbered n) propagating in the thickness/layer of the panels are calculated from the following relationship

$$v_p^n \approx 2d_1 \frac{f_p^n}{n},$$

Table 2: Velocities calculated from the frequency of the first longitudinal mode (f_{L_1}) and the recovered micropolar parameter K and the P-wave modulus (longitudinal modulus) M. The cut-off frequency is f_c.

Panel	density (kg/m^3)	d_1 (cm)	velocity ($\sqrt{\frac{M+\mathcal{K}}{\rho}}$) (m/s)	Velocity ($2f_{L_1}d_1$) (m/s)	f_c (Hz)
XPS	32	4	1229	1240	6000
XPS	32	2	1066	1064	6250
EPS	12	2	645	660	2171
EPS	12	3	602	600	3071
EPS	12	4	620	640	2242

where d_{th} is the panel thickness, f_p^n is the frequency of the nth mode determined from the transmission coefficient. Velocity can also be computed once the theoretical TC data is fitted to the experimental TC and found satisfactory. The following relationships engaging the mechanical moduli and density $v_p^1 = \sqrt{\frac{M+\mathcal{K}}{\rho}}$ from the theoretical model is employed.

Knowledge of the cut-toff frequency f_c and the phase velocity are important for determining the bounds of J. The expression for the phase velocity is rewritten as $(v_p^1)^2 = (M + 2\pi^2\rho\, J\, f_c^2)$. This shows that the velocity of the longitudinal modes also depend on the micropolar parameter J (the micro-inertia) among others. The measured and recovered phase velocities are in good agreement (difference < 4 percent) and are summarized in Table (2).

The influence of the Cosserat elastic constants and Poisson ratio on the transmission coefficient

The Sensitivity of the transmission coefficient vis-à-vis the micropolar parameters $\mathcal{K}$, J, γ and the Poisson ratio was studied by varying them while all the others remained fixed at their expected values. Their influence was analyzed by examining the changes occurring on the magnitude of the transmission coefficient as parameters were varied. It was observed that $\mathcal{K}$ (the Cosserat couple modulus), influenced the magnitude of the transmission coefficient (Fig. (8)a and c) over the whole range of frequencies. The changes in magnitude of the TC with the variations of $\mathcal{K}$ were found to be well marked. This was accompanied by a directly proportional increase/decrease of the resonance

frequency of the modes and as a consequence an advantage over the classical elastic model that has only two tuning parameters (E and ν). From this observation, the parameter $\mathcal{K}$ can easily be recovered from experimental data since it has a significant influence on the TC. The rotational inertia J and the twist coefficient γ influence the amplitudes around the zoomed area of Figs. 8a and b. This is around the cut-off frequency area. Therefore these two parameters can be considered as low frequency parameters. Poisson ratio was also found to influence the TC (Figs. 8d)

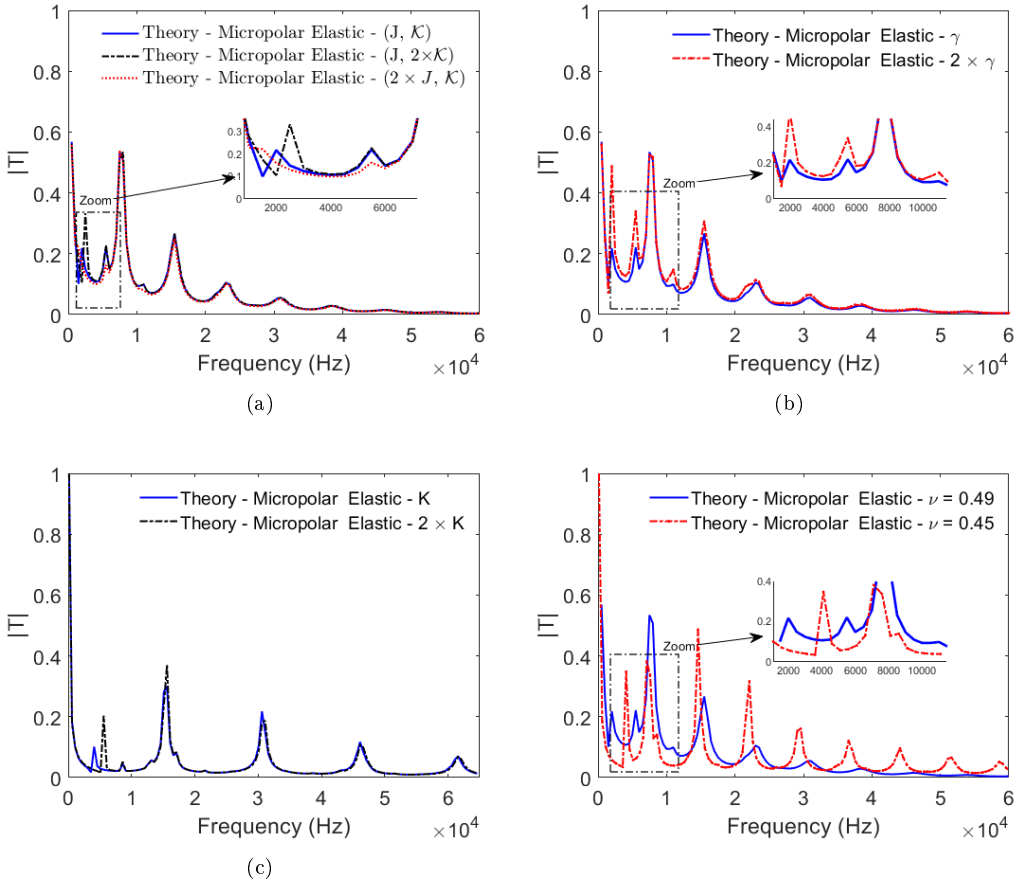

Figure 8: Sensitivity of the transmission coefficient to the variations of (a) The Cosserat couple modulus $\mathcal{K}$ ($\mathcal{K}$ = 42 kPa) and the rotational inertia $J = 4.7 \times 10^{-5}$ N/m and (b) The twist coefficient $\gamma = 5.6 \times 10^5$ N for an EPS12 4.0 cm thick panel. For the XPS 4.0 cm thick panel (c) Variation of $\mathcal{K}$ ($\mathcal{K}$ = 51 kPa). (d) Variation of Poisson ratio ν.

It is worth noting that the characteristic length [39, 40] can be obtained from the micropolar twist (γ) and couple ($\mathcal{K}$) modulus. This length is equal to the spherical polystyrene bead diameter size that forms the EPS12 foam (their diameters are usually in the range 0.3mm - 4mm). It is an intrinsic dimension defining the heterogeneous structure of the material. The characteristic length in bending in micropolar theory was given by Yang et al [39], as $l_{b2} = [\gamma/(2(2\mu + \mathcal{K}))]^{1/2}$ in mm. In reference [41], $\mathcal{K}$ in l_{b2} was neglected. The beads from the 4cm thick Eps12 foam had several diameters ranging from ≈ 0.3 mm to 4mm. The calculations with the recovered values herein gave $l_{b2} \approx 0.7$ mm.

4.3. Comparison between the theoretical micropolar elastic and classical elastic model

The micropolar model reproduces most of the small but different peaks (frequency and amplitude) at the beginning of the transmission coefficient (around the cut-off frequency) and in the higher modes (Fig. 7). The transmission coefficients of the theoretical micropolar elastic (modeling of an XPS 4cm thick panel) and that of the classical elastic continuum model and experiment were compared. The classical model was implemented using the Transfer matrix method (TMM) in which the longitudinal and shear modes were taken into account [32]. Both formulations capture the resonance peaks in the experimental TC curve (Fig. 9a). The absence of J in the classical elastic model was simulated to examine the effect of its absence on the TC of the micropolar elastic model. It was given a very small value, $J = 1 \times 10^{-50}\,\mathrm{Nm}^{-1}$ (J cannot be zero, it is denominator in the expressions for ω_0, c_3 and c_4). The connection between the two theories is more involved than merely making $J \to 0$ [14]. The resulting TC had a peak around the cut-off frequency missing (Fig. 9b).

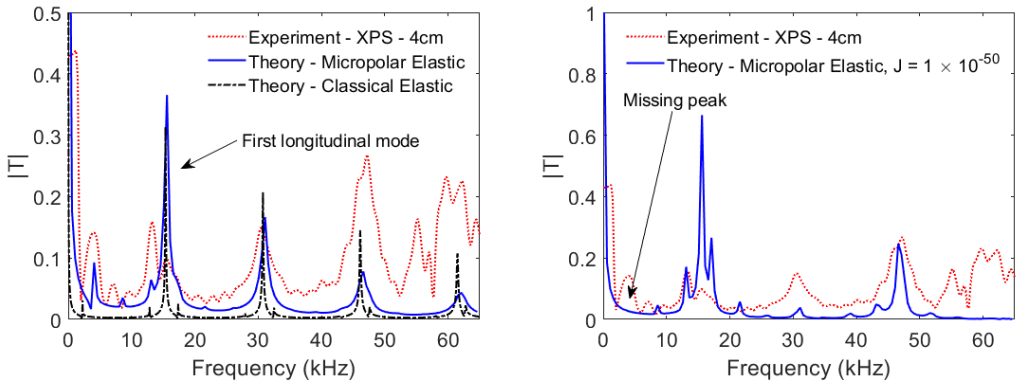

Figure 9: Comparison between the transmission coefficients for an XPS, 4.0 cm thick panel. (a) modeled by the micropolar elastic and the classical elastic formulations using the same E and ν. (b) The experimental and theoretical micropolar elastic model with a very small rotational inertia value, $J = 1.0 \times 10^{-50}$ N/m.

5. Conclusion

An experimental test rig was setup for the obtention of the transmission coefficient in *air* to recover the micropolar elastic properties of XPS and EPS panels in the audible and ultrasonic frequency ranges. Not only did the transmission coefficients agree with the theoretical ones but the elastic parameters also agreed well with those in the literature for EPS12 of the same density but obtained using a different measurement technique.

It was confirmed for the materials tested (two families of closed-cell polystyrene foams, XPS and EPS) that the Cosserat continuum model, which admits additional degrees of freedom associated with rotation of the microstructure, described best their behavior. It is a better alternative to the classical continuum model. The absence of transmission at the cut-off frequency and a better correspondence of the transmitted modes with the experiment, were found to be the main features that differentiates the micropolar elastic material behavior from the classical elastic one. These features were more marked in the transmission coefficient curves for the thicker EPS and XPS foams.

The Cosserat couple modulus, $\mathcal{K}$, the micro-inertia J and the twist modulus γ were found to influence the transmission coefficient of XPS and EPS thick plates in air. This

is an important finding because it implies that micropolar parameters: the micro-inertia J and $\mathcal{K}$ can be recovered using the measurement method developed herein. Recall that, only M and ν can be recovered using the classical elastic continuum theory [32].

Finally, this new method appeals to the characterization of closed-cell porous panels and will provide elasticity data especially for the XPS foams that are hard to come by in the available literature.

Declaration of Competing Interest

The authors declare that they have no known competing financial interests or personal relationships that could have appeared to influence the work reported in this paper.

Appendix A. The dispersion relationships

Plane wave type of propagation is assumed for which the potentials take the following forms

$$(q, \xi, \boldsymbol{\Pi}, \boldsymbol{\Theta}) = (\bar{q}, \bar{\xi}, \bar{\boldsymbol{\Pi}}, \bar{\boldsymbol{\Theta}}) \exp\left[\mathrm{i}(\boldsymbol{k} \bullet \boldsymbol{r} - \omega t)\right], \tag{A.1}$$

where $\boldsymbol{k}$ is the wave-number vector ($\boldsymbol{k} = k_x\hat{x} + k_y\hat{y} + k_z\hat{z}$), $\boldsymbol{r}$ the position vector ($\boldsymbol{r} = x\hat{x} + y\hat{y} + z\hat{z}$), $\bar{q}$,$\bar{\xi}$ are complex amplitude constants, while $\bar{\boldsymbol{\Pi}}$, $\bar{\boldsymbol{\Theta}}$ are complex vectors.

By using the vector identities in Appendix B and also writing $\nabla \times \boldsymbol{\Pi} = \mathrm{i}\,\boldsymbol{k} \times \boldsymbol{\Pi}$, Eqn. (4) can be written

$$(\omega^2 - k^2 c_2^2)\bar{\boldsymbol{\Pi}} + \mathrm{i}\,\frac{J\omega_0^2}{2}\,\boldsymbol{k} \times \bar{\boldsymbol{\Theta}} = 0, \qquad \mathrm{i}\frac{\omega_0^2}{2}\boldsymbol{k} \times \bar{\boldsymbol{\Pi}} + (\omega^2 - \omega_0^2 - c_4^2 k^2)\bar{\boldsymbol{\Theta}} = 0. \tag{A.2}$$

The dispersion relation is found through elimination of $\bar{\boldsymbol{\Pi}}$ and $\bar{\boldsymbol{\Theta}}$ from these equations

$$\bar{\boldsymbol{\Theta}} = \frac{-\mathrm{i}\omega_0^2}{2\left(\omega^2 - \omega_0^2 - c_4^2 k^2\right)}\,\boldsymbol{k} \times \bar{\boldsymbol{\Pi}} \Rightarrow (\omega^2 - k^2 c_2^2)\bar{\boldsymbol{\Pi}} + \frac{J\omega_0^4}{4\left(\omega^2 - \omega_0^2 - c_4^2\, k^2\right)}\,\boldsymbol{k} \times \boldsymbol{k} \times \bar{\boldsymbol{\Pi}} = 0 \tag{A.3}$$

Developing the expression $\boldsymbol{k} \times \boldsymbol{k} \times \bar{\boldsymbol{\Pi}} = (\boldsymbol{k} \bullet \bar{\boldsymbol{\Pi}})\bar{\boldsymbol{\Pi}} - (\boldsymbol{k} \bullet \boldsymbol{k})\bar{\boldsymbol{\Pi}} = -k^2\,\bar{\boldsymbol{\Pi}}$ (using the identity $\boldsymbol{A} \times (\mathbf{B} \times \boldsymbol{C}) = (\boldsymbol{A} \bullet \boldsymbol{C})\boldsymbol{B} - (\boldsymbol{A} \bullet \boldsymbol{B})\boldsymbol{C}$ and $\boldsymbol{k} \bullet \bar{\boldsymbol{\Pi}} = \boldsymbol{k} \bullet \bar{\boldsymbol{\Theta}} = 0$) then

$$k^4 + \left(\frac{{\omega_0}^2}{{c_4}^2}\left(1 - \frac{J\,\omega_0^2}{4\,{c_2}^2}\right) - \frac{\omega^2}{{c_2}^2}\left(1 + \frac{{c_2}^2}{{c_4}^2}\right)\right)k^2 + \frac{\omega^2}{{c_2}^2{c_4}^2}\left(\omega^2 - {\omega_0}^2\right) = 0.$$

which can also be written as a quartic equation of the type with solutions

$$k^4 - 2\,b\,k^2 + c = 0, \quad \Rightarrow \quad k_{3,4}^2 = -b \pm \sqrt{b^2 - 4\,c}, \tag{A.4}$$

where $b = \frac{\omega^2}{2\,{c_2}^2}\left(1 + \frac{{c_2}^2}{{c_4}^2}\right) - \frac{{\omega_0}^2}{2\,{c_4}^2}\left(1 - \frac{J,\omega_0^2}{4\,{c_2}^2}\right)$, $c = \frac{\omega^2}{{c_2}^2{c_4}^2}\left(\omega^2 - {\omega_0}^2\right)$

The two wave numbers, k_3 and k_4 are solutions and correspond to a transverse acoustic mode (TA-mode) and transverse Optic mode (TO mode). The upper sign (+) in the equation of the coupled transverse displacement wave corresponds to k_3; the lower sign (-) corresponds to the wave number k_4 of the coupled transverse microrotational waves.

Appendix B. Some vector calculus identities employed

The following vector calculus identities were employed

$$\nabla \bullet (\nabla \mathbf{q}) = \nabla^2 q,\, \nabla \bullet (\nabla \times \boldsymbol{\Pi}) = 0, \tag{B.1}$$

$$\nabla \times (\nabla q) = 0, \nabla \times (\nabla \times \boldsymbol{\Pi}) = \nabla(\nabla \bullet \boldsymbol{\Pi}) - \nabla^2 \boldsymbol{\Pi} \tag{B.2}$$

References

[1] E. Cosserat, F. Cosserat, Théorie des corps déformables, Librairie Scientifique, Hermann, Paris, 1909.

[2] W. Voigt, Theoretische studien fiber die elastizitatsverhiltnisse der kristalle (theoretical studies on the elasticity relationships of crystals), Abh. Gesch. Wissenschaften (1887) 34.

[3] R. A. Toupin, Elastic materials with couple-stresses, Arch. Rational Mech. Ana. 11 (1962) 385–414.

[4] R. D. Mindlin, H. F. Tiersten, Effects of couple-stresses in linear elasticity, Arch. Rational Mech. Ana. 11 (1962) 415–488.

[5] W. T. Koiter, Couple-stresses in the theory of elasticity, in: Pt. I-II. Proc. Koninkl., Neterland Akad., Wetensh B67, 1964, pp. 17–44.

[6] A. C. Eringen, Theory of micropolar elasticity, in: H. Liebowitz (Ed.), Fracture, Academic Press, New York, 1968, pp. 621–729.

[7] A. R. Hadjesfandiari, G. F. Dargush, Couple stress theory for solids, Int. J. Solids Struct. 48 (18) (2011) 2496–2510.
URL https://www.sciencedirect.com/science/article/pii/S0020768311001727

[8] M. Brand, M. Rubin, A constrained theory of a cosserat point for the numerical solution of dynamic problems of non-linear elastic rods with rigid cross-sections, Int. J. Nonlin. Mech. 42 (2) (2007) 216–232, special Issue in Honour of Dr Ronald S. Rivlin.
URL https://www.sciencedirect.com/science/article/pii/S0020746206000849

[9] A. C. Eringen, E. S. Suhubi, Elastodynamics, Vol. 2., Vol. Vol. 2, Academic Press, New York, 1975, Ch. 5.

[10] A. C. Eringen, Linear theory of micropolar elasticity, J. Math. Mech. 15 (6) (1966) 909–923.

[11] C. Kafadar, A. Eringen, Micropolar media-i the classical theory, Int. J. Eng. Sci. 9 (3) (1971) 271 – 305.
URL http://www.sciencedirect.com/science/article/pii/0020722571900401

[12] R. Mindlin, Stress functions for a cosserat continuum, Int. J. Solids Struct. 1 (3) (1965) 265 – 271.
URL http://www.sciencedirect.com/science/article/pii/0020768365900338

[13] J. Altenbach, H. Altenbach, V. A. Eremeyev, On generalized Cosserat-type theories of plates and shells: a short review and bibliography, Arch. Appl. Mech. 80 (1) (2010) 73–92.
URL https://doi.org/10.1007/s00419-009-0365-3

[14] S. Hassanpour, G. R. Heppler, Micropolar elasticity theory a survey of linear isotropic equations, representative notations, and experimental investigations, Math. Mech. Solids 22 (2) (2017) 224–242.
URL https://doi.org/10.1177/1081286515581183

[15] S. Duan, W. Wen, D. Fang, A predictive micropolar continuum model for a novel three-dimensional chiral lattice with size effect and tension-twist coupling behavior, J. Mech. Phys. Solids 121 (2018) 23 – 46.
URL http://www.sciencedirect.com/science/article/pii/S0022509618303016

[16] A. Spadoni, M. Ruzzene, Elasto-static micropolar behavior of a chiral auxetic lattice, J. Mech. Phys. Solids 60 (1) (2012) 156 – 171.
URL http://www.sciencedirect.com/science/article/pii/S0022509611001864

[17] R. S. Lakes, R. L. Benedict, Noncentrosymmetry in micropolar elasticity, Int. J. Eng. Sci. 20 (10) (1982) 1161 – 1167.

URL http://www.sciencedirect.com/science/article/pii/0020722582900969

[18] R. Kumar, S. K. Tomar, Reflection and transmission of elastic waves at viscous liquid-micropolar elastic solid interface, Int. J. Math. Math. Sci. 26 (11) (2001) 685–694.
URL http://dx.doi.org/10.1155/S0161171201005415

[19] D. Singh, S. Tomar, Longitudinal waves at a micropolar fluid/solid interface, Int. J. Solids Struct. 45 (1) (2008) 225 – 244.
URL http://www.sciencedirect.com/science/article/pii/S0020768307003071

[20] A. C. Eringen, Microcontinuum Field Theories - I. Foundations and Solids, 1st Edition, Classical and Continuum Physics, Springer-Verlag New York, New York, USA, 1999.

[21] R. Lakes, W. J. Drugan, Bending of a cosserat elastic bar of square cross section: Theory and experiment, J. Appl. Mech. 82 (9) (2015) 091002–091010.
URL http://dx.doi.org/10.1115/1.4030626

[22] H. Park, R. Lakes, Cosserat micromechanics of human bone: Strain redistribution by a hydration sensitive constituent, J. Biomech. 19 (5) (1986) 385 – 397.
URL http://www.sciencedirect.com/science/article/pii/0021929086900151

[23] R. Lakes, Experimental microelasticity of two porous solids, Int. J. Solids Struct. 22 (1) (1986) 55 – 63.
URL http://www.sciencedirect.com/science/article/pii/0020768386901034

[24] R. D. Gauthier, W. E. Jahsman, A quest for micropolar elastic constants, J. Appl. Mech. 42 (2) (1975) 369–374.
URL http://dx.doi.org/10.1115/1.3423583

[25] R. Lakes, Strongly Cosserat elastic lattice and foam materials for enhanced toughness, Cell. Polym. 12 (1993) 17–30.

[26] W. B. Anderson, , R. S. Lakes, Size effects due to Cosserat elasticity and surface damage in closed-cell polymethacrylimide foam, J. Mater. Sci. 29 (24) (1994) 6413–6419.
URL https://doi.org/10.1007/BF00353997

[27] ASTM C165-07(2012), Standard Test Method for Measuring Compressive Properties of Thermal Insulations, American Society for Testing and Materials (ASTM) International, West Conshohocken, PA (2012).

[28] ASTM D6817 D6817M 15, Standard Specification for Rigid Cellular Polystyrene Geofoam, American Society for Testing and Materials (ASTM) International, West Conshohocken, PA (2015).

[29] V. R. Parfitt, A. C. Eringen, Reflection of plane waves from the flat boundary of a micropolar elastic half-space, J. Acoust. Soc. Am. 45 (5) (1969) 1258–1272.
URL https://doi.org/10.1121/1.1911598

[30] A. C. Eringen, Microcontinuum Field Theories: I. Foundations and Solids, Springer New York,

2012.

[31] J. M. Carcione, Wave Fields in Real Media, 1st Edition, Vol. 31 of Handbook of Geophysical Exploration Seismic Exploration, Pergamon, Amsterdam, 2001.

[32] E. Ogam, Z. Fellah, G. Ogam, Identification of the mechanical moduli of closed-cell porous foams using transmitted acoustic waves in air and the transfer matrix method, Compos. Struct. 135 (2016) 205 – 216.

[33] L. J. Gibson, M. F. Ashby, Cellular solids : Structure and properties, 2nd Edition, Cambridge Solid State Science, Cambridge University Press, 1997.

[34] I. MathWorks, Signal Processing Toolbox for Use with MATLAB: User's Guide, version 7.2 (r2016a) Edition, Computation, visualization, programming, The MathWorks, Natick, MA USA, 2016.

[35] A. Nuttall, Some windows with very good sidelobe behavior, IEEE Trans. Acoust., Speech, Signal Process. 29 (1) (1981) 84–91.

[36] E. Ogam, Z. Fellah, N. Sebaa, J.-P. Groby, Non-ambiguous recovery of Biot poroelastic parameters of cellular panels using ultrasonic waves, J. Sound Vib. 330 (6) (2011) 1074 – 1090.
URL http://www.sciencedirect.com/science/article/pii/S0022460X10006371

[37] Y. Beju, J. Mandal, Expanded polystyrene (eps) geofoam: Preliminary characteristic evaluation, Procedia Eng. 189 (2017) 239 – 246, proceedings of the International Scientific Conference Transportation Geotechnics and Geoecology (TGG-2017).
URL http://www.sciencedirect.com/science/article/pii/S1877705817321598

[38] ASTM D1621 - 10, Standard Test Method for Compressive Properties Of Rigid Cellular Plastics, American Society for Testing and Materials (ASTM) International, West Conshohocken, PA (2010).

[39] J. Yang, R. S. Lakes, Experimental study of micropolar and couple stress elasticity in compact bone in bending, Journal of Biomechanics 15 (2) (1982) 91–98.
URL https://www.sciencedirect.com/science/article/pii/0021929082900409

[40] F.-Y. Huang, B.-H. Yan, J.-L. Yan, D.-U. Yang, Bending analysis of micropolar elastic beam using a 3-D finite element method, International Journal of Engineering Science 38 (3) (2000) 275–286.
URL https://www.sciencedirect.com/science/article/pii/S0020722599000415

[41] Z. Rueger, R. S. Lakes, Cosserat elasticity of negative poisson's ratio foam: experiment, Smart Materials and Structures 25 (5) (2016) 054004.
URL https://doi.org/10.1088/0964-1726/25/5/054004